Analysis and Determination of Nickel Plasma Parameters: Using the LIBS Technique and Statistical Analysis with SPSS Software

Muna Ahmed Issa[1], Zina Mahmood Shaban[1], Tahseen Hussain Mubarak[2], Shaymaa A. Hussein[3], Sami Salman Chiad[1], Nadir Fadhil Habubi[1, 4, 5] and Yassin Hasan Kadhim[6]
[1]*Department of Physics, College of Education, Mustansiriyah University, 10052 Baghdad, Iraq*
[2]*Department of Physics, College of Science, University of Diyala, 32001 Diyala, Iraq*
[3]*Department of Medical Laboratory Techniques, Al-Manara College for Medical Sciences, 62001 Amarah, Iraq*
[4]*Department of Radiation and Sonar Technologies, Alnukhba University College, 10001 Baghdad, Iraq*
[5]*Department of Radiology Techniques, Al-Qalam University College, 36001 Kirkuk, Iraq*
[6]*Department of Optics Techniques, College of Health and Medical Techniques, Al-Mustaqbal University, 51001 Hillah, Iraq*
dr.sami@uomustansiriyah.edu.iq

Keywords: Nickel Plasma, Plasma Parameters, LIBS Technique, Statistical Analysis, SPSS.

Abstract: In this work, the spectral imaging technique, involving the application of a high-energy laser pulse to a nickel sheet, was employed along with the Debye length and the number of particles in the Debye sphere. The results showed that increasing the laser energy from 400 to 800 mJ led to an increase in electron temperature from 0.262 to 0.323 eV, an increase in electron density from 5.00×10^{18} cm^{-3} to 5.50×10^{18} cm^{-3}, a slight increase in plasma frequency from 2.008×10^{13} Hz to 2.106×10^{13} Hz, and an increase in the Debye length from 1.699×10^{-6} cm to 1.802×10^{-6} cm. The number of particles in the Debye sphere was significantly greater than one, thus fulfilling the condition for the presence of a true plasma. Statistical analysis using SPSS software was used to confirm the results through descriptive analysis, correlation, and regression. The findings demonstrated that the standard deviation of the plasma parameters was slight, and the correlations confirmed a strong positive relationship between laser energy, temperature, and electron density. In contrast, the Eigen-to-Eigen correlation between Debye length and laser energy was weaker. The regression analysis showed that plasma parameters are strongly dependent on laser energy. In contrast, the Debye length may depend on other parameters.

1 INTRODUCTION

Laser-induced breakdown spectroscopy (LIBS) is an analytical method that uses spectra from a pulsed laser-excited plasma on a sample [1]. LIBS was conducted extensively in a range of fields and applications [2]. This is due to its ability to analyze small specimens, detect in real time, be user-friendly, and detect remotely. LIBS has gained popularity over the past few years and is commonly used across diverse fields [3]. It is also linked to simple and inexpensive devices [4]. Using certain types of lasers with different targets, you can analyze the sample in real time. Since then, LIBS has been widely applied in many areas for the determination of product elemental composition [5], biomedical [6], environmental [7], geological [8], and mineral mining processes [9]. Laser irradiation produces nickel plasma, which remains of particular interest because nickel is a valuable element for various industrial, catalytic, and electronic uses [10]. In that which we present, we see that study of nickel plasma from laser irradiation's point of view adds to the knowledge of plasma formation dynamics, energy transfer mechanisms, and emission features for LIBS based diagnosis and material processing which we see play out in different laser settings [11]. Also of great import is the role of statistics in the interpretation of data and in the validation that the plasma parameters we obtain are reliable and consistent. While statistics is a science in it's own right statistics is not to be reduced to just numbers. Statistics includes a set of data which is true but statistics as a field also looks at the what we may call the science behind the data the why and how of it [12]. We also look at statistics as a tool for data analysis which includes the use of graphs and tables for prediction and hypothesis testing [13].

Also in this work we put forth to use LIBS to study and diagnose the plasma we see from laser induced nickel plasma, and to also put the results through the p ringer so to speak of descriptive and inferential statistics in SPSS. This method allows the correct interpretation of experimental data, the correlation between laser energy and plasma parameters, and the confirmation of the statistical significance of the observed results.

2 EXPERIMENTAL

In Figure 1, the LIBS emission spectrum of nickel plasma generated in air is shown. The plasma was fabricated by a Q-switched Nd: YAG laser with a wavelength of 1064 nm, a pulse duration of 9 ns, a pulse frequency of 6 Hz, and different pulse energies of 400, 600, and 800 mJ, chosen to span a range of ablation regimes while maintaining stable plasma formation and avoiding excessive plasma shielding at the target surface. A concentrated laser beam was concentrated on the titanium particle at an incidence angle of 45°. The titanium plasma plume expanded above the target surface upon irradiation. Plasma light from irradiation was collected with an optical fiber at 45° to the target surface to capture additional signals and minimize geometric losses. The emission was sent to the spectrometer, where the LIBS spectra were recorded and analyzed by a computer. Statistical analysis was performed using SPSS version 25 to determine the rates and standard deviations of the plasma parameters, assess their correlation, and fit linear regression models to predict their behaviour.

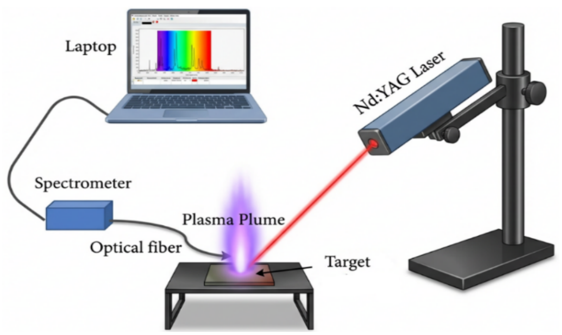

Figure1: The LIBS for the Nickel plasma system setup.

3 RESULTS AND DISCUSSION

LIBS analysis relies on the interaction between a laser pulse and the material to be analyzed and follows the principle outlined in Figure 2. A laser beam is focused on the sample's surface, depositing significant energy in a short time. Then, a sudden heating of the samples results in ablation and vaporization. The vapor absorbs a portion of laser radiation [14]. The form is a plasma with electrons, atoms, and ions in an excited state. This sets up all these mechanisms both during and after the laser pulse (just a few µs) [15]. The laws of quantum mechanics govern laser-matter interaction, explaining how photons are absorbed or emitted by atoms [16]. The different energy levels of each type of atom, with narrow-band emissions due to quantization, and one uncertainty known as Heisenberg's uncertainty principle [17]. It is these emissions that give rise to spectral emission lines present in LIBS spectra, their properties, and the associated energy levels for each atom [18]. For example, while travelling through ambient atmosphere, both atoms and ions emit photons with wavelengths characteristic of the emitting atomic elements. Thus, by extracting radiation from plasma, the spectrum can be analyzed to recognize the elements in plasma and, by extension, in the analyzed sample, using databases of observed emission lines [19]. The radiation is collected through an optical fiber connected to a spectrometer coupled to a detector [20]. In this work, plasma from a nickel target is detected using LIBS at laser energies (E_L) of 400 mJ, 600 mJ, and 800 mJ. The spectrum of observed emission sources was determined by correlating the spectral peaks observed with information from the NIST database to assign atomic and ionic Ni emission lines accurately (Ni I and Ni II) [21]. A significant rise in the intensity of emission lines is also observed as the laser energy is ramped up, presumably due to higher ablation rates, increased electron heating, and better excitation and ionization processes in nickel plasma due to greater effective coupling of laser energy to matter [22]. The transition probabilities and statistical weights of selected electronic transitions determine the line intensities at different wavelengths. Furthermore, since ionization is comparatively low in the circumstances under which this work is conducted, the emission intensities of the neutral nickel species are relatively higher than those of the ionic species [23].

The electron temperature (T_e) and electron density (n_e) are necessary thermodynamic quantities in plasma that must be accounted for. The plasma temperature has a physical significance only within Local Thermodynamic Equilibrium (LTE) [24]. The Boltzmann-Plot is also shown in Figure 3. The Boltzmann plot is expressed as (1) [25],

$$\text{Ln}\left(\frac{I_{ji}\lambda_{ji}}{A_{ji}g_{ji}}\right) = \frac{E_j}{k_B T_e} + C. \quad (1)$$

Where I_{ji}, λ_{ji}, and A_{ji} are intensity, wavelength and transition probability, respectively, corresponding to the transition from j to i, g_j is a statistical weight, K_B is Boltzmann constant, E_j is the energy of the upper excited level j. The nine wavelength set was used as a parameter to estimate T_e. These nine lines were selected on the basis of their high intensity, minimal self-absorption, and wide range of upper energy levels, which together ensure accurate Boltzmann plot analysis. They were computed using standard Ni-I lines from NIST (Table 1).

Table 1: The NIST data of Ni-I lines that were used in the Boltzmann plot.

Λ (nm)	Intensity	A_{ji}. $g_j \times 10^8$	lower level (eV)	upper level (eV)
300.249	1255.17	5.60	0.02539	4.15357
305.082	733.793	5.40	0.02539	4.08818
310.155	1177.93	4.40	0.109083	4.10541
336.957	2452.41	1.30	0.0000	3.67848
341.476	2838.62	5.00	0.02539	3.65518
345.847	3321.38	3.00	0.212396	3.79632
351.505	2838.62	2.90	0.109083	3.63531
356.637	695.172	2.80	0.422778	3.89827
361.939	1602.76	4.60	0.422778	3.84736

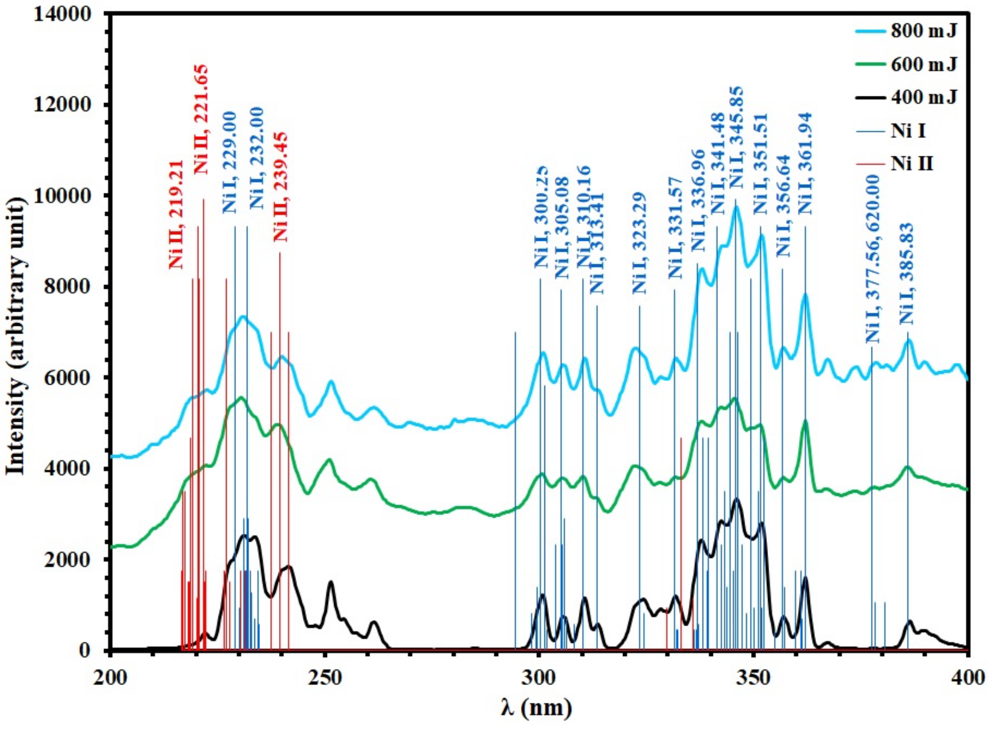

Figure 2: LIBS for Ni target in atmospheric air.

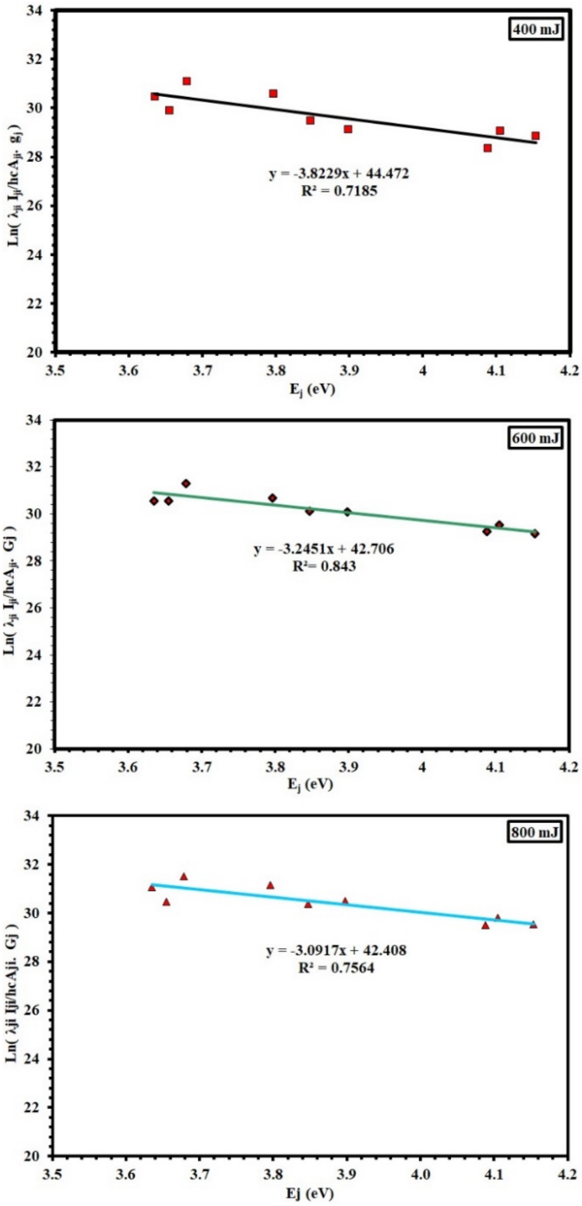

Figure 3: Boltzmann plot of Ni-I lines for LIBS using 1064 nm.

The Ni emission line at 361.9 nm, recorded at different laser energies, is shown in Figure 4, with the best Lorentzian-fitting profiles. As the laser energy increases, spectral line broadening becomes noticeable [26]. Such behaviour is attributed to an enhanced laser–plasma interaction, which leads to higher ablation rates and improved plasma plume confinement. This increases electron density; therefore, the emission line profiles are widest due to Stark broadening [27]. ne was calculated using the Stark broadening method as in (2) [28].

$$n_e = \left[\frac{\Delta\lambda_{FWHM}}{2\omega}\right] N_r. \quad (2)$$

Where: $\Delta\lambda_{FWHM}$ is the full width at half maximum of the line, ω and is the theoretical line full-width Stark broadening parameter, which is computed at the same reference electron density $N_r=10^{16}$ (cm^{-3}).

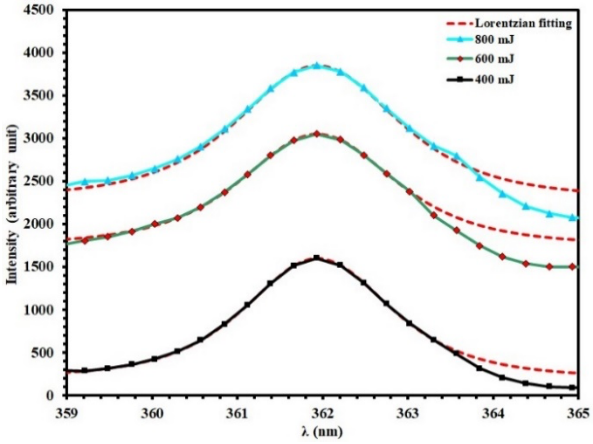

Figure 4: Ni-I 361.9 nm line profiles and its Lorentzian fitting in air.

Figures 5 and 6 show the responses of T_e and n_e to E_L. The results indicated saturation/slow variation of n_e and T_e. The noticed behaviour relates to plasma shielding effect (PSE), i.e., its reflection of laser light. PSE of air limits ionization and reduces the accessible laser intensity for mass ablation [29].

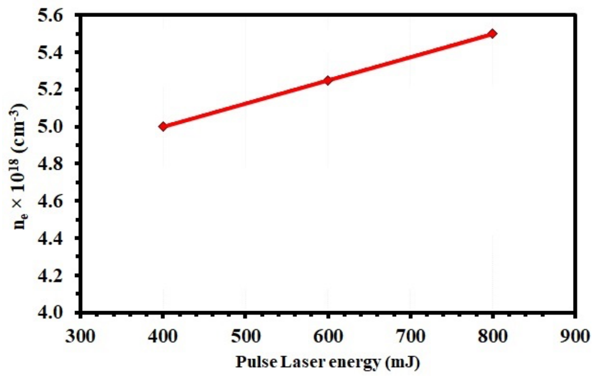

Figure 5: Relation between Te and the different laser energies for Ni-plasma.

Figure 7 and 6 shows the changes in plasma frequency (f_p) and Debye length (λ_D) with laser energy across 400–800 mJ. Clearly, as the laser energy rises, plasma frequency increases, while Debye length decreases. The plasma frequency grows with laser energy in a uniform manner physically, as f_p is linearly related to the n_e in (3) [30].

$$f_p\ (\mathrm{Hz}) = 8.98 \times 10^3 \sqrt{n_e}\,. \quad (3)$$

The additional electron density at higher laser energies leads to stronger collective plasma oscillations and thus a higher plasma frequency [11]. the Debye increases slightly at higher energies, as shown in Figure 8. This is because the rise in T_e at the same time promotes the thermal motion of electrons. Since λ_D depends on both T_e and n_e, as expressed in (4) [31].

$$\lambda_D = \sqrt{\frac{\varepsilon_0 K_B T_e}{n_e e^2}}. \quad (4)$$

Where: ε_0 is the permittivity of free space, e is electron charge, resulting in a marginal increase in λ_D. Such behavior has been documented in [32].
The number of particles in the Debye sphere (N_D) reflects the second criterion for plasma presence $N_D >> 1$; it depends on n_e and λ_D, (5) [33]-[35]:

$$N_D = \frac{4\pi}{3} n_e \lambda_D^3. \quad (5)$$

A significant value of N_D indicates that many charged particles are contained within the Debye sphere, ensuring effective electrostatic shielding and confirming the validity of plasma conditions. The obtained values are much greater than unity for all investigated laser energies, confirming the formation of a stable and well-defined laser-induced plasma. In the present study, all calculated plasma parameters are summarized in Table 2.

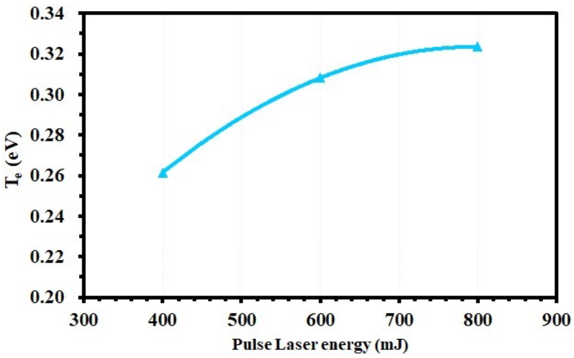

Figure 6: Relation between ne and the different laser energies for Ni-plasma.

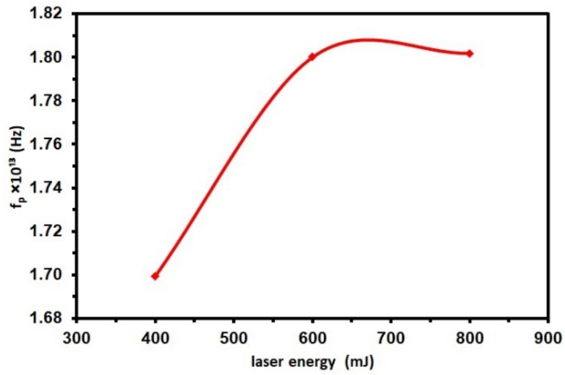

Figure 7: Relation between fp and the different laser energies for Ni-plasma.

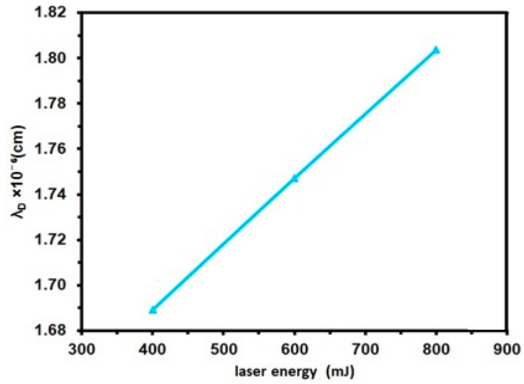

Figure 8: Relation between □D and the different laser energies for Ni-plasma.

3.1 Statistical Analysis

Statistical analysis was performed to validate the replicability and reliability of the plasma response. A quantitative assessment of trends in plasma parameters with laser energy was conducted using descriptive statistics, correlation analysis, and linear regression to ensure that the observed variations were systematic rather than random.

Table 2: Plasma parameter for Ni- Plasma at distinct laser energies.

E (mJ)	T_e (eV)	$\Delta\lambda$ (nm)	$n_e \times 10^{18}$ (cm^{-3})	$f_p \times 10^{13}$ (Hz)	$\lambda_D \times 10^{-6}$(cm)	N_D
400	0.262	2.00	5.00	2.008	1.699	103
600	0.308	2.10	5.25	2.058	1.800	128
800	0.323	2.20	5.50	2.106	1.802	135

3.1.1 Descriptive Statistics

1- I entered the experimental data into SPSS version 25 (Fig. 9). Descriptive statistical analysis was then performed to obtain the means and standard deviations of the plasma parameters. This was done through the following path:

Analyze → Descriptive Statistics → Descriptives (Fig. 10).

It is the case that we did descriptive analysis which was a result of the small number of experimental points.

In Table 3 we present the results.

Table 3: Output of stats report.

Parameter	Mean	Std. Deviation
T_e (eV)	0.2977	0.03179
FWHM (nm)	2.1000	0.10000
n_e (cm)	5.2500	0.25000
f_p (Hz)	2.0573	0.04900
λ_D (cm)	1.7670	0.05890
N_D	122.0000	16.82260

SPSS based descriptive statistics report that we see the development of stable and well defined plasma characteristics within the studied laser energy range. Mean electron temperature we report at 0.2977 eV which has very little standard deviation which in turn reports very consistent and efficient electron heating under high laser irradiation. Also we see that spectral line broadening has only small variation around an average of 2.10 nm which in large part reports that the plasma excitation conditions do not change. Stark broadening used to determine the electron density which we report an average of 5.25 x 10^18 cm^-3 with low dispersion which we attribute to uniform plasma formation and improved ionization at high laser energies. Also the plasma frequency does what we see in electron density which in turn we put forth as proof of the diagnostic approach's reliability. Also we note very short Debye length at 1.767 x 10^-6 cm which reports effective electrostatic screening within the plasma. Also the Debye number (N_D 122) which is by large greater than unity reports the establishment of a true plasma state for all experimental conditions.

3.1.2 Correlation Analysis

In the present study input energy was used for the x axis and plasma parameters which include Te, ne, fp, λD, and ND were put on the y axis. We looked at the relationship between x and y which is reported via a correlation coefficient we denote as "r". The value of "r" range between -1 and +1. We report our results of Correlation Analysis in Table 4. Figure 11 and 12 presents Pearson correlation analysis via SPSS.

Table 4 reports the Pearson correlation between laser energy (E_l) and the primary plasma parameters. We see that there is a very strong positive correlation between laser energy and spectral line broadening (FWHM), electron density (n_e), and plasma frequency (f_p) (r 1.000, p 0.01 for all) which in turn means that as we increase laser energy these parameters go up in proportion. Also we note a great positive correlation between laser energy and electron temperature (r 0.960) which in turn confirms that we see greater plasma heating at higher laser energies; physically, this increase in Te and ne with laser energy is attributed to enhanced inverse-bremsstrahlung absorption and more efficient coupling of laser energy into the plasma, which raises the ablation rate and the degree of ionization. Also the Debye number which we look at has a very large positive trend with laser energy (r 0.951) which in turn reflects that we see more intense particle interactions and larger scale plasma behavior. Although slightly lower, the correlation between laser energy and Debye length remains positive (r = 0.874), suggesting that while it is influenced by laser energy, it is also affected by other plasma characteristics such as temperature and charge density [36]-[38].

3.1.3 Regression Analysis

Linear regression captures the relationship between two variables. This is a modeling approach that predicts the reliant variable from one or more autonomous variables [39]-[40]. In the present work, the relationships among E_L, T_e, n_e, FWHM, f_p, λ_D, and N_D are studied. The work appears as Figure 13 in SPSS [41]-[43].

Table 5 and 6 show the Model Summary and Coefficients, which include the important information of correlation coefficient (R), coefficient of determination (R^2), standard error, and B constant.

The linear regression results for the plasma parameters are presented in Table 7. The regression analysis reveals a strong linear relationship between laser energy and electron temperature, characterized by a high correlation coefficient (R = 0.960) and a coefficient of determination ($R^2 = 0.921$), indicating that approximately 92.1% of the variation in electron temperature is explained by changes in laser energy [44]-[47]. The low standard error of the estimate (0.01266 eV) [47]-[51], which we report shows that the put forth linear model is very accurate and reliable, we also note that the trend of increased electron temperature is very much a consistent and systems as we increase laser energy [52]-[55].

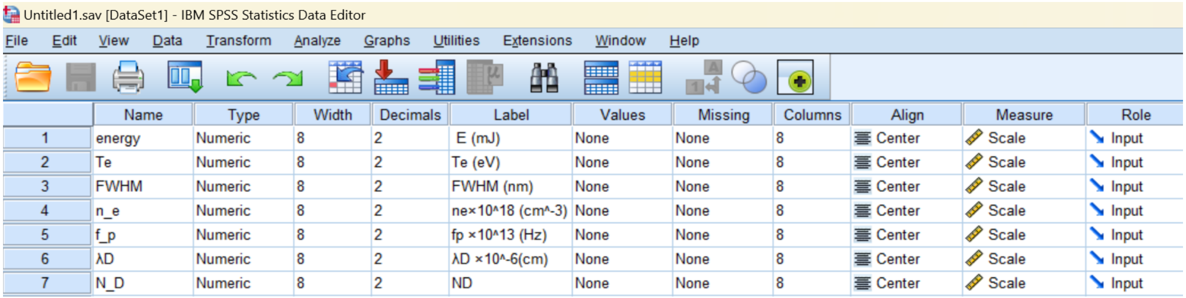

Figure 9: SPSS view variable data.

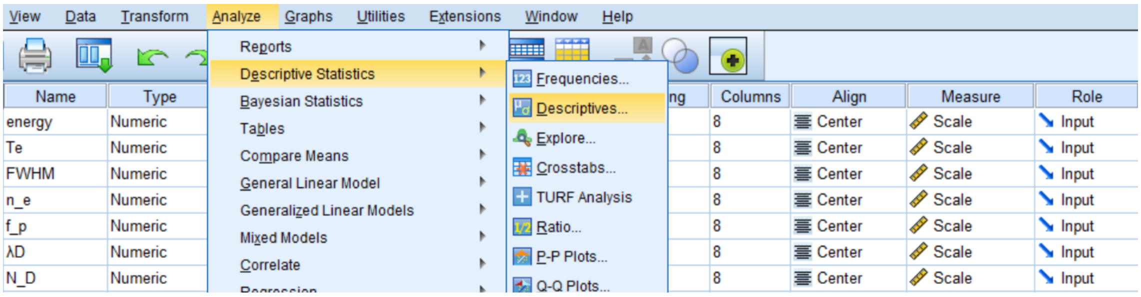

Figure 10: Steps to access descriptive statistics in SPSS version 25.

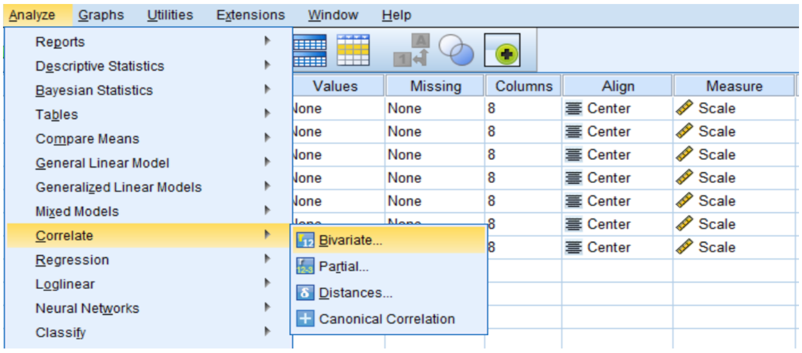

Figure 11: First step: access the Pearson correlation analysis menu in SPSS version 25.

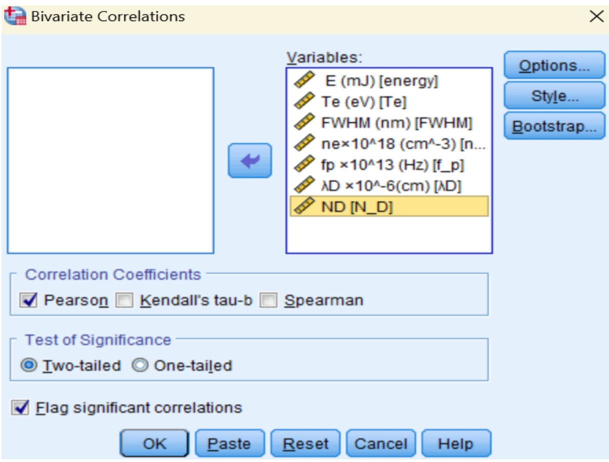

Figure 12: Second Step: access the Pearson correlation analysis menu in SPSS version 25.

Table 4: Results of Correlation Analysis between EL and plasma parameters.

Correlations								
		E (mJ)	Te (eV)	FWHM (nm)	n_e (cm)	f_p (Hz)	λ_D (cm)	N_D
E (mJ)	Pearson Correlation	1	.960	1.000**	1.000**	1.000**	.874	.951
T_e (eV)		.960	1	.960	.960	.963	.976	1.000*
FWHM (nm)		1.000**	.960	1	1.000**	1.000**	.874	.951
n_e (cm)		1.000**	.960	1.000**	1	1.000**	.874	.951
f_p (Hz)		1.000**	.963	1.000**	1.000**	1	.880	.955
λ_D (cm)		.874	.976	.874	.874	.880	1	.982
N_D		.951	1.000*	.951	.951	.955	.982	1
**. Correlation is significant at the 0.01 level (2-tailed).								
*. Correlation is significant at the 0.05 level (2-tailed).								

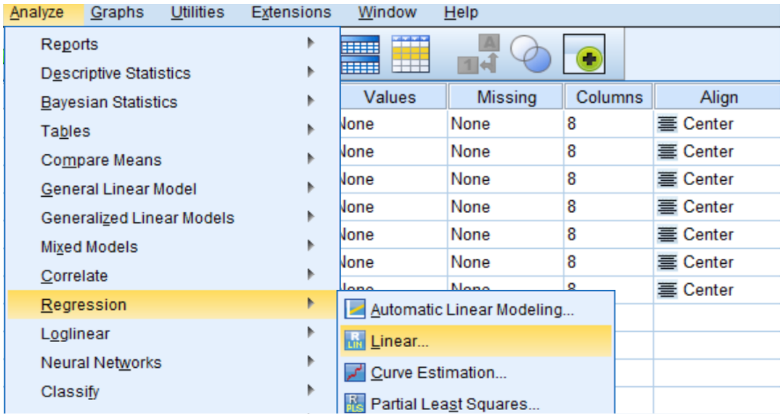

(a)

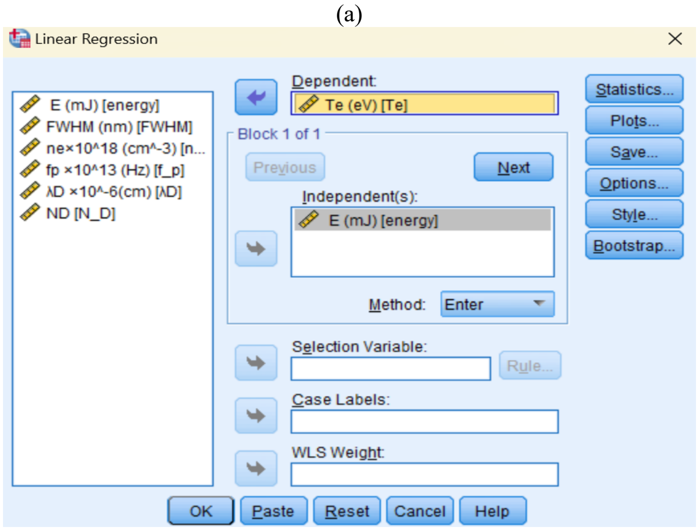

(b)

Figure 13: Steps for performing linear regression analysis in SPSS Statistics version 25: a) accessing the Linear Regression Analysis menu and b) configuring the analysis. The same procedure was repeated for the remaining plasma parameters.

Table 5: Model summary in SPSS to Energy and Te.

Model Summary				
Model	R	R Square	Adjusted R Square	Std. Error of the Estimate
1	.960[a]	.921	.841	.01266
a. Predictors: (Constant), E (mJ)				
b. Dependent Variable: T_e (eV)				

Table 6: Coefficients in SPSS to Energy and Te.

Coefficients								
Model		Unstandardized Coefficients		Standardized Coefficients	t	Sig.	95.0% Confidence Interval for B	
		B	Std. Error	Beta			Lower Bound	Upper Bound
1	(Constant)	.206	.028		7.410	.085	-.147-	.560
	E (mJ)	.000	.000	.960	3.408	.182	.000	.001

Table 7: For plasma parameters which also includes linear regression.

Plasma parameter	(R)	(R^2)	the standard error	B constant
FWHM (nm)	1	1	0.00	1.8
n_e (cm)	1	1	0.00	4.500
f_p (Hz)	1	1	0.00082	1.910
λ_D (cm)	0.874	0.765	0.04042	1.613
N_D	0.951	0.905	7.32847	74.00

The regression model which describes this relationship is:

$$T_e = 0.206 + 0.00015E.$$

This relation reports that laser energy is directly proportional to electron heating which we see via the positive slope, also we note that the small error in measurement reports stable plasma behavior across the investigated energy range. We apply the same regression analysis to the other plasma parameters which in turn enables the development of a large scale model which includes R, R^2, standard error, and regression coefficients; this in turn is put toward predictive analysis of plasma characteristics [56]-[58].

In our analysis we note that change of FWHM, electron density (n_e) and plasma frequency (f_p) is found to be complete function of laser energy which accounts for a 100% of their variable over the looked at range. On the other hand we see that the Debye number is very much a large player of laser energy which for about 90.5% of it's fluctuation. Also we find that the Debye length reports a moderate correlation and that which 76.5% of that variable is due to the laser energy. From these results we see that laser energy is the main player in plasma excitation, ionization processes and collective behavior. Also the partial role of the Debye length into play which which means that other plasma elements like temperature and particle interactions also play a role in it's variation in different plasma states [59]-[62].

4 CONCLUSIONS

In this work we used Laser Induced Breakdown Spectroscopy (LIBS) which we applied to a nickel target via high energy laser pulse irradiation. We also looked at base plasma parameters which included electron temperature (T_e), electron density (n_e), Debye length, and number of particles in the Debye sphere and reported on what we found. We present that laser based methods put forth a practical, economic and environmental solution for plasma diagnosis. We noted that as laser power increased plasma characteristics did in particular we saw great change in T_e and n_e which also played a large role in the other parameters' behavior. Using SPSS for our stats we report low standard deviation which in turn reports high stability and reproducibility of the plasma states. Also we saw that the plasma parameters are very much so related to each other. Regression analysis also supported that the put forward plasma parameters' great sensitivity to laser power input which in turn reports the efficiency of LIBS in the control of plasma character assessment.

ACKNOWLEDGMENTS

Mustansiriyah University financially supported this research through its institutional academic research program.

REFERENCES

[1] G. Lu, L. Sun, Z. Cong, and T. Chen, "Study on laser-induced breakdown spectroscopy in high-pressure helium gas environment for deep ocean applications," Talanta, vol. 270, Art. no. 125531, 2024.

[2] M. A. Issa and K. A. Aadim, "Study the structural and optical properties of Zinc Oxide prepared by pulse laser deposition," Journal of Optics, pp. 1-6, 2024.

[3] C. Ghany, K. M. Lee, H. K. Sanghapi, and V. K. Singh, "Diagnostics of Laser-Induced Plasma," in Laser Induced Breakdown Spectroscopy (LIBS): Concepts, Instrumentation, Data Analysis and Applications, vol. 1, pp. 45-64, 2023.

[4] M. A. Issa and K. A. Aadim, "Influence Of Laser Energy On Structural And Optical Properties Of ZnO(x):NiO(1−x) Films Prepared By Pulse Laser Deposition," Journal of Optics, pp. 1-7, 2024.

[5] Z. J. Kamil, M. J. Zoory, and H. J. Mohamad, "LIBS technique for plant mineral ratio analysis and environmental and agricultural importance: a comprehensive review," The European Physical Journal D, vol. 78, no. 3, p. 27, 2024.

[6] A. V. Skalny, T. V. Korobeinikova, M. Aschner, O. V. Baranova, E. G. Barbounis, A. Tsatsakis, and A. A. Tinkov, "Medical application of laser-induced breakdown spectroscopy (LIBS) for assessment of trace element and mineral in biosamples: Laboratory and clinical validity of the method," Journal of Trace Elements in Medicine and Biology, vol. 79, Art. no. 127241, 2023.

[7] T. K. Sankar, Abhilash, and P. Meshram, "Environmental impact assessment in the entire life cycle of lithium-ion batteries," Reviews of Environmental Contamination and Toxicology, vol. 262, no. 1, p. 5, 2024.

[8] G. S. Senesi and R. S. Harmon, "Application of LIBS to terrestrial geological research," in Laser Induced Breakdown Spectroscopy (LIBS): Concepts, Instrumentation, Data Analysis and Applications, vol. 2, pp. 593-614, 2023.

[9] V. Balaram, "Advances in analytical techniques and applications in exploration, mining, extraction, and metallurgical studies of rare earth elements," Minerals, vol. 13, no. 8, p. 1031, 2023.

[10] A. G. Ramu, M. A. Kumari, J. Theerthagiri, D. Choi, and M. Y. Choi, "Metal nanoparticles and alloys produced by pulsed laser irradiation in liquids for water splitting," in Pulsed Laser-Induced Nanostructures in Liquids for Energy and Environmental Applications, Elsevier, pp. 177-191, 2024.

[11] Y. Liu, C. Wu, L. Dong, and J. Xiu, "Multi-dimensional analysis of NiCr alloy nanofilms based on Ps-LIBS technology," Spectrochimica Acta Part B: Atomic Spectroscopy, vol. 222, Art. no. 107062, 2024.

[12] T. Weiland and I. Williams, "Culturally relevant data in teaching statistics and data science courses," Journal of Statistics and Data Science Education, vol. 32, no. 3, pp. 256-271, 2024.

[13] D. Shete and P. Khobragade, "An empirical analysis of different data visualization techniques from statistical perspective," in AIP Conference Proceedings, vol. 2839, no. 1, Art. no. 040017, 2023.

[14] A. K. Pathak, N. K. Rai, A. Singh, A. K. Rai, P. K. Rai, and P. K. Rai, "Medical applications of laser induced breakdown spectroscopy," in Journal of Physics: Conference Series, vol. 548, no. 1, Art. no. 012007, IOP Publishing, 2014.

[15] M. Leprince, L. Sancey, J. L. Coll, V. Motto-Ros, and B. Busser, "L'imagerie élémentaire par spectroscopie LIBS-De nouvelles applications en médecine," médecine/sciences, vol. 35, no. 8-9, pp. 682-688, 2019.

[16] J. Kaiser, K. Novotný, M. Z. Martin, A. Hrdlička, R. Malina, M. Hartl, et al., "Trace elemental analysis by laser-induced breakdown spectroscopy-Biological applications," Surface Science Reports, vol. 67, no. 11-12, pp. 233-243, 2012.

[17] F. Anabitarte, A. Cobo, and J. M. Lopez-Higuera, "Laser-induced breakdown spectroscopy: fundamentals, applications, and challenges," International Scholarly Research Notices, vol. 2012, no. 1, Art. no. 285240, 2012.

[18] J. A. Aguilera and C. Aragón, "Characterization of laser-induced plasmas by emission spectroscopy with curve-of-growth measurements. Part II: Effect of the focusing distance and the pulse energy," Spectrochimica Acta Part B: Atomic Spectroscopy, vol. 63, no. 7, pp. 793-799, 2008.

[19] M. Rashid, H. A. Anwar, M. S. Aslam, and A. Rashid, "Laser-induced breakdown spectroscopy for soil analysis: Recent advances in nutrient and contaminant detection," Spectrum of Engineering Sciences, pp. 279-288, 2025.

[20] B. Jean-Marc, "Faire la lumière sur les mystères du sous-sol avec… de la lumière. Lumière dans les Sciences de l'Ingénieur," Polytech-News, vol. 55, p. 21, 2017.

[21] NIST National Institute of Standards and Technology (USA), Electronic database.

[22] L. Torrisi, F. Caridi, D. Margarone, and L. Giuffrida, "Nickel plasma produced by 532-nm and 1064-nm pulsed laser ablation," Plasma Physics Reports, vol. 34, no. 7, pp. 547-554, 2008.

[23] N. Bolouki, J. H. Hsieh, C. Li, and Y. Z. Yang, "Emission spectroscopic characterization of a helium atmospheric pressure plasma jet with various mixtures of argon gas in the presence and the absence of de-ionized water as a target," Plasma, vol. 2, no. 3, pp. 283-293, 2019.

[24] E. Thimsen, "Beyond equilibrium thermodynamics in the low temperature plasma processor," Journal of Vacuum Science & Technology B, vol. 36, no. 4, 2018.

[25] M. Issa and K. A. Aadim, "Influence of gas flow rate on the plasma temperature and electron density of an atmospheric argon plasma jet," Jordan Journal of Physics, vol. 18, no. 4, pp. 435-442, 2025.

[26] Z. Yang, B. Tang, Y. Qiu, J. Wu, W. Wei, X. Huang, et al., "Measurement of transient temperature using laser-induced breakdown spectroscopy (LIBS) with the surface temperature effect," Journal of Analytical Atomic Spectrometry, vol. 38, no. 10, pp. 1952-1961, 2023.

[27] J. Wu, Y. Zhou, M. Chen, and X. Li, "Numerical modeling and simulation on nanosecond laser-target interactions," Journal of Physics D: Applied Physics, vol. 58, no. 14, Art. no. 143004, 2025.

[28] A. J. Ghazai, O. M. Abdulmunem, K. Y. Qader, S. S. Chiad, and N. F. Habubi, "Investigation of some physical properties of Mn doped ZnS nano thin films," in AIP Conference Proceedings, vol. 2213, no. 1, Art. no. 020101, 2020.

[29] T. A. Khalepha and N. K. Abdalameer, "Comparative analysis of plasma generated using LIBS technique for different wavelengths of pulsed laser of a cadmium target," Baghdad Science Journal, vol. 21, no. 12 (Suppl.), pp. 4128-4139, 2024.

[30] H. A. Hussin, R. S. Al-Hasnawy, R. I. Jasim, N. F. Habubi, and S. S. Chiad, "Optical and structural properties of nanostructured CuO thin films doped by Mn," Journal of Green Engineering, vol. 10, no. 9, pp. 7018-7028, 2020.

[31] S. N. Mazhir and H. H. Abbas, “Influence of pulse laser energy on the Nickel plasma characteristics that produced in laser-induced plasma system,” Baghdad Science Journal, vol. 21, no. 5, p. 1684, 2024.

[32] K. Qu, S. Meuren, and N. J. Fisch, “Signature of collective plasma effects in beam-driven QED cascades,” Physical Review Letters, vol. 127, no. 9, Art. no. 095001, 2021.

[33] N. I. Rahayu, M. Muktiarni, and Y. Hidayat, “An application of statistical testing: A guide to basic parametric statistics in educational research using SPSS,” ASEAN Journal of Science and Engineering, vol. 4, no. 3, pp. 569-582, 2024.

[34] K. Kumari and S. Yadav, “Linear regression analysis study,” Journal of the Practice of Cardiovascular Sciences, vol. 4, no. 1, pp. 33-36, 2018.

[35] N. Roustaei, “Application and interpretation of linear-regression analysis,” Medical Hypothesis, Discovery and Innovation in Ophthalmology, vol. 13, no. 3, p. 151, 2024.

[36] M. Vasudeva, S. D. Varalakshmi, S. D. George, and V. K. Unnikrishnan, “Engineered liquid-repellent substrate for enhanced Laser-Induced Breakdown Spectroscopy (LIBS) of liquid samples,” Applied Surface Science, Art. no. 166364, 2026.

[37] B. Xue, W. Sun, Y. Bai, Z. Wang, C. Chen, X. X. Li, et al., “Laser energy modulation in laser-induced breakdown spectroscopy of marine aerosols: unraveling energy-coupling pathways and improving quantitative analysis,” Journal of Analytical Atomic Spectrometry, 2026.

[38] Y. You, B. Xue, and J. Riedel, “Enhancement of LIBS plasma in air with organic solvent vapors,” Spectrochimica Acta Part B: Atomic Spectroscopy, vol. 236, Art. no. 107309, 2026.

[39] J. Li, Y. Zhang, C. Zhang, D. He, X. Cheng, and J. Bai, “Gas or bulk?- size effect of aerosol particles in interaction with laser-induced plasma,” Optics & Laser Technology, vol. 193, Art. no. 114245, 2026.

[40] A. P. Sreekala, D. B. Mora, M. B. de la Mora Mojica, J. Y. T. Sánchez, V. Contreras, and C. Sánchez-Aké, “Laser-induced breakdown spectroscopy of water-dispersed gold nanoparticles in acoustically levitated droplets: Parameter adjustment for enhanced signal,” Spectrochimica Acta Part B: Atomic Spectroscopy, Art. no. 107483, 2026.

[41] H. Enayati-Taloobaghi, S. Soltani, M. M. Shahidi, and E. Salahi, “Phase engineering and UV photoresponse of TiO_2 films on Si substrates modified with spatially distributed Au nanoparticles,” Journal of Materials Science: Materials in Electronics, vol. 37, no. 2, p. 155, 2026.

[42] C. Z. Eldjilali, G. S. H. Thien, Z. N. Ng, B. K. Yap, K. B. Tan, H. A. Murthy, and K. Y. Chan, “Electrochromic performances of TiO2 nanocrystals thin films for smart glass applications,” Thin Solid Films, vol. 815, Art. no. 140636, 2025.

[43] M. K. Rashid, H. J. Mohammed, H. M. Hameed, M. W. Muayad, A. M. Hussien, A. T. Awad, and M. Alharbi, “The effect of titanium dioxide (TiO_2) nanoparticle concentration on the performance of polycrystalline silicon solar cells,” Journal of Umm Al-Qura University for Engineering and Architecture, vol. 16, no. 4, pp. 1753-1764, 2025.

[44] R. Özmenteş and A. S. Hassanien, “Characterizations and optical discussions of thermally evaporated titanium dioxide thin films,” Journal of Optics, vol. 54, no. 3, pp. 1322-1340, 2025.

[45] A. M. Al Saleh, “A Review of the Synthesis, Structural, and Optical Properties of TiO2 Nanoparticles: Current State of the Art and Potential Applications,” Crystals, vol. 15, no. 11, p. 944, 2025.

[46] İ. Erol, G. Khamidov, R. Uktamjon, T. Davlat, and S. Tillayev, “Enhanced thermal, dielectric, and antimicrobial performance of fluorinated methacrylate and chitosan-based nanocomposites reinforced with TiO2 nanowires,” Cellulose, vol. 32, no. 16, pp. 9429-9450, 2025.

[47] M. A. Issa and K. A. Aadim, “Optical and structural characterization of ZnO:NiO nano composite prepared by pulsed laser deposition method,” Journal of Optics, vol. 54, pp. 2357-2362, 2025.

[48] M. L. Vera, H. D. Traid, A. N. Dwojak, M. R. Rosenberger, and C. E. Schvezov, “Advances in nanostructured TiO2 coatings for industrial applications,” in Industrial Applications of Nanoparticles, CRC Press, pp. 228-255, 2023.

[49] K. Nagaraj, S. Radha, C. G. Deepa, K. Raja, V. Umapathy, N. P. Badgujar, et al., “Photocatalytic advancements and applications of titanium dioxide (TiO_2): Progress in biomedical, environmental, and energy sustainability,” Next Research, vol. 2, no. 1, Art. no. 100180, 2025.

[50] N. Farooq, P. Kallem, Z. ur Rehman, M. I. Khan, R. K. Gupta, T. Tahseen, et al., “Recent trends of titania (TiO2) based materials: A review on synthetic approaches and potential applications,” Journal of King Saud University-Science, vol. 36, no. 6, Art. no. 103210, 2024.

[51] N. S. Kamarudin, N. N. Yaakob, N. F. Sukor, H. D. Setiabudi, M. A. H. Aziz, and R. Jusoh, “Dual-Role Deep Eutectic Solvent-Assisted Electrosynthesis of TiO_2/KCC-1 for Enhanced Visible-Light Photocatalytic Desulfurization,” Arabian Journal for Science and Engineering, pp. 1-20, 2026.

[52] W. Zhao, H. Jia, J. Qu, C. Yang, Y. Wang, J. Zhu, et al., “Sol-gel synthesis of TiO2-SiO2 hybrid films with tunable refractive index for broadband antireflective coatings covering the visible range,” Journal of Sol-Gel Science and Technology, vol. 107, no. 1, pp. 105-121, 2023.

[53] M. O’Byrne, B. Kerzabi, M. Abbarchi, A. Lifschitz, T. Zamora, V. Malgras, et al., “Investigation of the anatase-to-rutile transition for TiO2 sol-gel coatings with refractive index up to 2.7,” Thin Solid Films, vol. 790, Art. no. 140193, 2024.

[54] A. Saeed, E. Alzahrani, M. A. Morsi, A. E. Tarabiah, E. M. Abdelrazek, S. Aldwais, et al., “Enhanced optical and electrical properties of PEO/PMMA/TiO2 nanocomposites for optoelectronic applications,” Optical Materials, vol. 157, Art. no. 116402, 2024.

[55] F. Piccinno, F. Gottschalk, S. Seeger, and B. Nowack, “Industrial production quantities and uses of ten engineered nanomaterials in Europe and the world,” Journal of Nanoparticle Research, vol. 14, no. 9, p. 1109, 2012.

[56] S. Devi, N. Talreja, D. Chauhan, S. Sahu, and M. Ashfaq, "Bioresource-derived Propolis wrapping for ZnO/TiO_2 nanocomposites: A sustainable photo-antibiotic material," Inorganic Chemistry Communications, Art. no. 116270, 2026.

[57] S. N. Ogugua, O. M. Ntwaeaborwa, and H. C. Swart, "Latest development on pulsed laser deposited thin films for advanced luminescence applications," Coatings, vol. 10, no. 11, p. 1078, 2020.

[58] Olvera-Rodríguez, R. Hernández, A. Medel, C. Guzmán, L. Escobar-Alarcón, E. Brillas, et al., "TiO2/Au/TiO2 multilayer thin-film photoanodes synthesized by pulsed laser deposition for photoelectrochemical degradation of organic pollutants," Separation and Purification Technology, vol. 224, pp. 189-198, 2019.

[59] M. Dhankhar, O. P. Singh, and V. N. Singh, "Physical principles of losses in thin film solar cells and efficiency enhancement methods," Renewable and Sustainable Energy Reviews, vol. 40, pp. 214-223, 2014.

[60] H. H. Jaber, K. A. Aadim, and A. Boughariou, "Influence of laser energy on spectroacopic analysis and structural and optical properties of (CdTe)1−x:Snx thin films," Journal of Optics, pp. 1-10, 2024.

[61] Z. M. Abbas and Q. A. Abbas, "Characterization of Magnetized-Plasma System Induced by Laser," Iraqi Journal of Physics, vol. 21, no. 4, pp. 45-55, 2023.

[62] S. A. Abbas and S. N. Mazhir, "Spectroscopic investigation of Zn plasma induced by Nd:YAG laser," in AIP Conference Proceedings, vol. 3282, no. 1, Art. no. 050053, 2025.